Results in Physics 6 (2016) 851–859

Contents lists available at ScienceDirect

Results in Physics

journal homepage: www.journals.elsevier.com/results-in-physics

Yield surface evolution for columnar ice

Zhiwei Zhou, Wei Ma *, Shujuan Zhang, Yanhu Mu, Shunpin Zhao, Guoyu Li

State Key Laboratory of Frozen Soil Engineering, Cold and Arid Regions Environmental and Engineering Research Institute, Chinese Academy of Sciences, Lanzhou 730000, China

ARTICLE INFO

Article history:
Received 25 September 2016
Received in revised form 24 October 2016
Accepted 26 October 2016
Available online 28 October 2016

Keywords:
Columnar ice
Multiaxial loading
Hardening rule
Path dependency
Yield criterion

ABSTRACT

A series of triaxial compression tests, which has capable of measuring the volumetric strain of the sample, were conducted on columnar ice. A new testing approach of probing the experimental yield surface was performed from a single sample in order to investigate yield and hardening behaviors of the columnar ice under complex stress states. Based on the characteristic of the volumetric strain, a new method of defined the multiaxial yield strengths of the columnar ice is proposed. The experimental yield surface remains elliptical shape in the stress space of effective stress versus mean stress. The effect of temperature, loading rate and loading path in the initial yield surface and deformation properties of the columnar ice were also studied. Subsequent yield surfaces of the columnar ice have been explored by using uniaxial and hydrostatic paths. The evolution of the subsequent yield surface exhibits significant path-dependent characteristics. The multiaxial hardening law of the columnar ice was established experimentally. A phenomenological yield criterion was presented for multiaxial yield and hardening behaviors of the columnar ice. The comparisons between the theoretical and measured results indicate that this current model is capable of giving a reasonable prediction for the multiaxial yield and post-yield properties of the columnar ice subjected to different temperature, loading rate and path conditions.

Introduction

The strength of ice is an interest and important subject in field of materials and physics [1–12]. It is essential for practical applications, such as the stability of glacier [10,13], cold region engineering [14–18] and the ocean and offshore engineering [19–21]. The strength of ice relies strongly in its physical properties (porosity, grain size and fabric, imperfections and brine content), the temperature conditions and the loading process (loading rate, loading history, loading path, the orientation of loading with respect to the c axis of ice crystals). The earlier works were focused on the strength of ice as a function of the strain rate, temperature, grain size and other factors in simple stress state, i.e. uniaxial compression and tensile. It is generally accepted that the strength of ice increases as the decreasing of temperature and the increasing of strain rate, and the failure process of ice transforms from the ductile to brittle mode under this change conditions of temperature and strain rate. During this decade, the attention and interest of scholars was extended to study the mechanical property of ice, particularly strength and constitutive theory, damage process and mechanism, brittle-ductile transition condition, fracture and crack mechanism, under complex stress state such as triaxial compression, combined shear-compression and shear-tensile tests [10,11,19,22–27]. Before further discussion about the strength characteristics of ice, it is necessary to distinguish clearly between three different meanings (concepts) for this property of ice that corresponds completely to different failure mechanism of the material [28]. First is the fracture strength, which occurs under brittle conditions when a brittle crack is formed that propagates across an ice sample for a complete fracture. Second is the initial yield strength caused by the initial formation of internal cracking, and it occurs under ductile conditions such that the ice does not failure at this stress points but continues to deform with the increase of stress. This process does not result in complete failure of ice sample until the failure strength (third) corresponding to the peak stress is reached. In view of the importance of strength characteristics for engineering application, the multiaxial yield (failure) behavior of ductile and brittle ice has been investigated by many researchers for establishing the experimental yield surface and further proposing the corresponding yield criterion. Jones [29] carried out triaxial compression tests on the polycrystalline ice under broad range of strain rates and confined pressures. The experimental results indicated that the rise of failure strength is rapid with the increase of the confining pressure at first, the strength value then remain approximate

* Corresponding author.
E-mail address: mawei@lzb.ac.cn (W. Ma).

http://dx.doi.org/10.1016/j.rinp.2016.10.020
2211-3797/

constant with further increases of confined pressure. The failure strength increases linearly at strain rates of the range from 10^{-7}/s to 10^{-1}/s under constant confined pressure conditions. Nadreau and Michel [30] made an analysis on the Jones' experimental results [28], and applied the yield criteria of soil and rock to the isotropic ice for considering the phase change effects due to hydrostatic pressure. Based on the triaxial compression results of freshwater ice at low confining pressures, Nadreau et al. [31] extended further the previous failure criterion to the anisotropic ice and verified experimentally the applicability of this theoretical model at different strain rates. Timco and Freerking [32] performed the biaxial compression tests on the columnar sea ice, and an anisotropic failure criterion was established according to experiment failure envelopes obtained from three different stress planes. Smith and Schulson [33] used the saline columnar ice to conduct the biaxial proportional compression at the strain rate of 10^{-2}/s, and the loading plane is orthogonal to the columnar axes. The testing results showed that the proportional ratio is important parameter for brittle-ductile failure transition of the columnar ice, and the shape of brittle failure envelopes at temperature of −10 °C and −40 °C is consistent. Rist and Murrell [34] present the failure envelope for the isotropic fresh water ice by using a set of concentric elliptical curves in the p-q stress plane. The same the multiaxial failure model was proposed to predict the triaxial results of iceberg ice given by Gagnon and Gammon [35]. The major goal of this works is to determinate experimentally whether or not the same failure criterion can be used for both iceberg ice and fresh water isotropic ice. Derradji-Aouat [36] used the multi-surface failure theory to describe the multiaxial failure behaviors of the saline ice, the fresh water isotropic ice and iceberg ice. Experimental results indicated that the theory model is applicable to the failure of all three types of ice. The triaxial proportional compressions were also conducted on the saline ice for investigating the multiaxial anisotropic strength under different failure modes and the effect factors in the brittle and ductile transition [4,37,38]. Those yield criteria for other engineering materials were used to describe the multiaxial compression data of the ice sample. It is worth noting that the initial yield and failure strength of the ductile ice is based on the different definition method corresponding to the different mechanism of the microstructure variation, respectively [28,37].

It is well-known that the strength criterion of material is an important theoretical tool to characterize quantificationally the strength distribution under complex stress state, which is realistic working condition of engineering materials [39–43]. The existing literatures referring the strength criterion of ice is limited, as multiaxial loading tests under low temperatures are notoriously difficult to conduct. On the other hands, the hardening property of the ice, corresponding to subsequent yield behavior, is crucial for engineering design since that the ice structures may be under post-yield stress stare in practical conditions. However, relevant studies concerning the multiaxial post-yield behavior and subsequent yield surface of ice has been not reported by now. Therefore, this paper presents a new triaxial method of exploring multiaxial yield and hardening response of the columnar ice with two objectives in mind. The first purpose is to investigate the multiaxial yield and hardening behavior under different stress state, further establish the initial and subsequent yield surface of the columnar ice, and verified experimentally the evolution rule of subsequent yield surface under different stress path. The second aim is to present a simple but reliable phenomenological yield criterion for predicting the multiaxial yield and hardening behavior of the columnar ice. In addition, the effect of temperature, loading rate and loading path in the initial and subsequent yield surface of the columnar ice will be discussed in detail.

Sample preparation and experimental methods

The fresh-water columnar ice was prepared by applying the Laboratory-grown procedure (LGI) of Kuehn et al. [44]. It is effective and economical method to simulate and study the physical and mechanical properties of the ice according to the LGI procedure [4,20,44]. The tank is filled with filtered Lanzhou tap water equilibrated to near 0 °C. The ice samples were then formed by freezing downwards from the upper surface using a cooling plate attached to a circulating cold bath, which is the realistic freezing condition. The freezing block was cut and machined into cylindrical ice samples with approximately 125 mm in height and 62 mm in diameter, as shown in Fig. 1. The c-axes of this columnar ice sample were unaligned within the plane of the block (i.e., perpendicular to the growth direction) [42]. This crystallographic structure leads directly to the anisotropy mechanical properties. The density of ice sample is 0.88 ± 0.02 g/cm^3 at three temperature conditions (−1.5 °C, −3 °C and −5 °C). It should be pointed out that ice sample after tests expanded into a bucket shape (Fig. 1(b)) due to shear dilatancy behavior, but the radial deformation is still small. The diameter of the top and lower surface keeps within the scope of 62–62.5 mm after tests, and the diameter of the expoxy resin platen contacting with the top and lower surface of ice sample is 62.7 mm. Therefore, the top and lower surface of ice sample is always loading fully in the whole process, the stress state of the ice sample is considered to be uniform in this paper. Triaxial testing machine (shown in Fig. 2(a)), which is capable of measuring the volumetric strain of the ice sample, was used to investigate the strength and deformation properties of the freshwater columnar ice at the complex stress states. Fig. 2(b) shows a schematic of loading and temperature control systems for the triaxial testing machine. The overall loading system is consisted of the axial loading segment and confined pressure segment, and the axial loading process can be controlled by load and displacement respectively (shown in Fig. 2(c)). The axial load and displacement value, measured by the axial transducer, were used to calculate the axial stress and strain of the ice sample in the testing process. The maximum axial load is 100 kN, and the variation range of the axial displacement is from −85 cm to 85 cm. The aeronautic hydraulic oil is used in confining pressure system, and the range value of the available confining pressure is 0–25 MPa. The alcohol is used as cooling medium in the temperature control system, and the range value of testing temperature is from 0 °C to −30 °C. Based on the displacement of the axial piston and the oil cylinder piston in the testing, the volumetric strain of the ice sample can be calculated by the following formula:

$$\varepsilon_v = \frac{\Delta V}{V_0} = \frac{S_0(H_t - H_0) + S_a(h_t - h_0)}{V_0} \quad (1)$$

where V_0 is the original volume of the ice sample; S_a and S_0 are the cross-sectional areas of the axial piston and the oil cylinder piston, respectively (S_a = 30.2 cm^2, S_0 = 34 cm^2). h_t and h_0 are the original and current positions of the axial piston, respectively; H_t and H_0 are the current and initial positions of the oil cylinder piston, respectively. It worth noting that the calculated volume strain should include to the compression deformation of the hydraulic oil, pipeline system, as well as expoxy resin platen (as shown in Fig. 2(b)). Deformation quantity of piping system and hydraulic oil can be determined by the following method: the steel sample (the size is same to ice sample with 125 mm in height and 62 in diameter) is used to conduct to hydrostatic compression test. Due to large stiffness of the steel sample, the volume compression quantity is negligible under the hydrostatic pressure condition of 0–10 MPa. According to the equation 1, the volume strain under above-mentioned hydrostatic tests can be determined. Those

(a) (b)

Fig. 1. Columnar ice sample (a) before tests (b) after tests.

continuous volume strain value are caused by deformation quantity of hydraulic oil and piping system under the condition of continuous confining pressure (0–10 MPa). In triaxial tests, the real volume strain can be obtained by subtracting the amount of hydrostatic volume strain from measured volume strain corresponding to same confined pressure conditions. In addition, because that the stiffness of expoxy resin platen (E = 2.8 GPa to 3.5 GPa) is much larger than it of ice sample under testing temperatures, its deformation can be ignored within the testing confined pressure ranges from 0 to 10 MPa.

In order to investigate experimentally the yield and hardening behaviors under complex stress state, the triaxial tests were performed on the ice samples by utilizing different stress paths. It should be pointed out that the referred stress paths in this paper are discussed in the stress space of effective stress versus mean stress. For the sake of illustration convenience, the loading ratio η is introduced to define the stress paths:

$$\eta = \frac{d\sigma_e}{d\sigma_m} \tag{2}$$

$$\sigma_{\mathrm{m}} = \frac{1}{3} I_1 = (\sigma_1 + \sigma_2 + \sigma_3)/3 \tag{3}$$

$$\sigma_{\mathrm{e}} = \sqrt{3J_2} = \frac{1}{\sqrt{2}} \sqrt{(\sigma_1 - \sigma_2)^2 + (\sigma_2 - \sigma_3)^2 + (\sigma_3 - \sigma_1)^2} \tag{4}$$

The loading ratio η can be rewritten under axisymmetric stress condition:

$$\eta = \frac{d(\sigma_1 - \sigma_3)}{d(\frac{\sigma_1 + 2\sigma_3}{3})} \tag{5}$$

$$\eta' = \frac{d\sigma_1}{d\sigma_3} = \frac{1 + 2\eta/3}{1 - \eta/3} \tag{6}$$

The principal stress σ_1 and σ_3 is controlled independently by the axial loading system and confined pressure system, and the triaxial tests under different stress path were conducted by regulating the proportional ratio of η'. The loading ratio η = 0, 3 and 0–3, stand for the case of the hydrostatic test, the triaxial tests under different stress paths, respectively. For the purpose of exploring the yield surface evolution, the initial and subsequent yield surfaces of fresh-water ice were determined by testing each ice sample through the stress path sketched in Fig. 3. First, the ice sample was hydrostatically compressed until the isotropic compression yield point, as indicated by the path o → a in Fig. 3. Then, the pressure was decreased at a constant rate along stress path a → b, and an axial stress rate was applied until the axial strain had incremented by 0.5%, referred to as the path b → c. The axial load was then removed (c → d) and the pressure was decreased further (d → e) and the procedure was repeatedly performed (e → f → g → h). This testing procedure was continued until the hydrostatic pressure was decreased to zero. The similar procedure was also executed by starting at the uniaxial stress path and gradually building up the hydrostatic pressure in order to compare the experimental yield surfaces obtained by two loading methods. Multiaxial yield points, defined of axial strain 0.5% (detail discussion in "Results and discussion"), were summaried in the stress space of the mean stress versus the effective stress. The experimental yield surface of fresh-water ice at different temperatures (−1.5 °C, −3 °C and −5 °C), loading rates (V axial = 0.05, 0.1, 0.2 MPa/min) and loading paths (η = 1.5, 2, 3) conditions were probed respectively for further studying the effect of those factors in initial yield surface. Moreover, for constructing and analyzing the evolution law of the experimental yield surface,

(a)

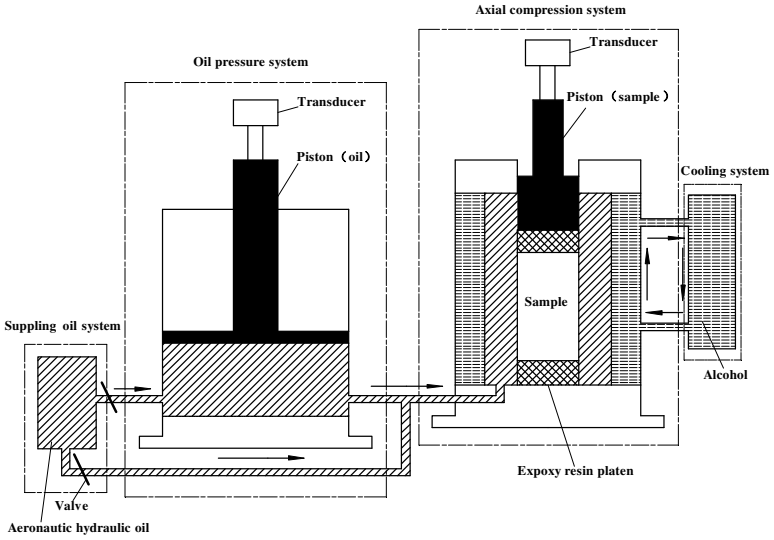

（b）

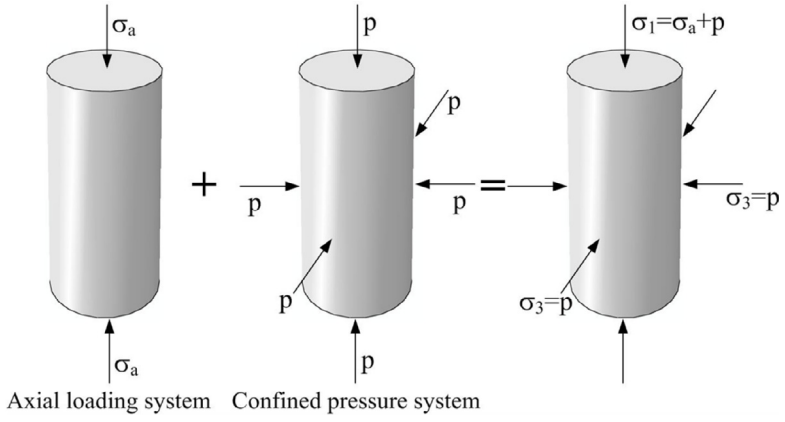

（c）

Fig. 2. Testing system. (a) A photograph of triaxial test apparatus. (b) A schematic of triaxial test apparatus. (c) Loading mode of ice sample.

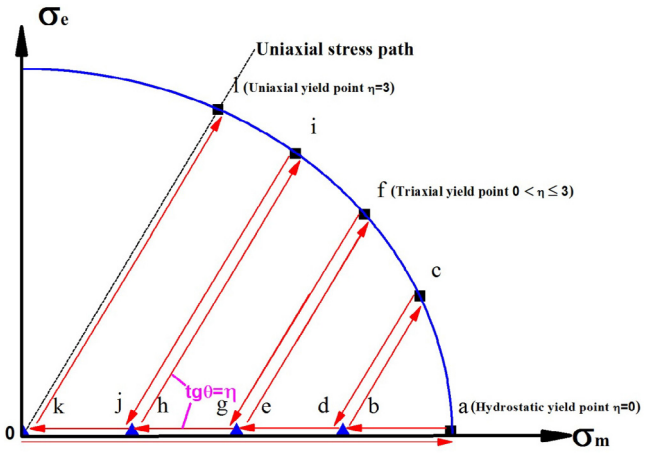

Fig. 3. Exploring for the experimental yield surface.

the subsequent yield surfaces under uniaxial and hydrostatic hardening conditions were established by using aforementioned method. The ice sample was firstly subjected to hydrostatic compression until a pre-strain (1%, 1.5%, 2% and 2.5%), and then the hydrostatic pressure was removed completely. The subsequent yield surface was re-determinated by repetition of testing procedure. The evolution process of the yield surface under hydrostatic path was determinated experimentally. The yield surface evolution under uniaxial path (axial strain 3%, 6%, 9% and 12%) was also characterized in a similar manner.

Results and discussion

Effective stress–axial strain curves and volumetric strain-axial strain curves of the columnar ice under different condition are shown in Fig. 4. The shape of curve under three temperatures and confine pressures is simple. Initially, the effective stress varies linearly with axial strain. After the onset of crushing at yield point, the slope of the curve gradually decrease due to the loss of stiffness. It is mainly attributed by the progressive crushing of pore microstructure and the propagation of initial crack in the ice sample. This behavior continues until the stress peak is reached, then the effective stress rapidly drops and remains at a nearly constant value as the axial strain increases. The volumetric strain-axial strain curve under different loading cases is yet simple. The curve is comprised of elastic and plastic parts: a linear compression stage, a peak strain point, a dilatancy stage where the volumetric strain decreases continuously as the ice sample deform plastically. The development of volumetric strain at the initial loading stage is corresponding to the compaction of the porosity in the ice sample (axial strain 0–2%), and the plastic strain occurs at the phase of the volume expansion (more than axial strain 0.5%). The peak points indicate that the weakest pore region starts to be crushed. The initial pore-distribution of the columnar ice is closely related to sample preparation process, and the compaction process must cause to the local deformation of sample. But this magnitude of local strain is limited by the porosity of the sample (1%–4%). This range value of the porosity does not lead to the large local strain in the loading process, the hypothesis for uniform deformation is effective and reasonable to the plastic behavior of ice sample. The change ratio of the volumetric strain decreases as the increase of the confined pressure at dilatancy stage. The primary contribution for this result is that the capacity of the radial plasticity deformation is restricted gradually since the increase of the confined pressure. On the basis of linear elastic characteristics of the volumetric strain, the Poisson's ratio of ice sample under initial compression region can be calculated by following equations:

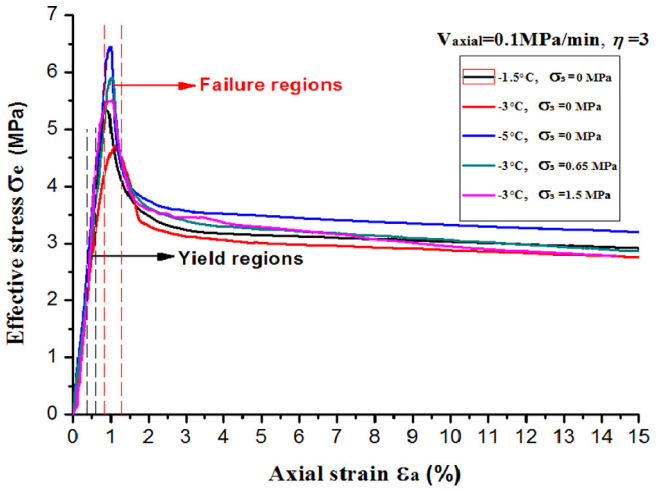

(a)

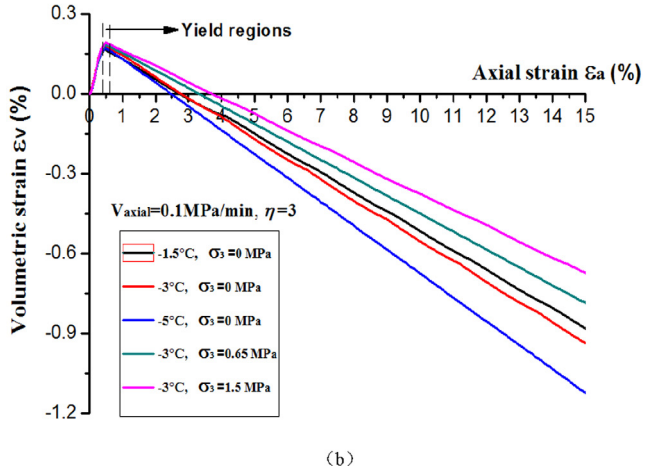

(b)

Fig. 4. Triaxial test results at different temperatures and confined pressures.

$$v(t) = -\frac{\varepsilon_3(t)}{\varepsilon_1(t)} = -\frac{[\varepsilon_v(t) - \varepsilon_1(t)]/2}{\varepsilon_1(t)} \tag{7}$$

$$v_{mean} = \frac{\int_0^{t_0} v(t)dt}{t_0 - 0} = \frac{\int_0^{t_0} \left[1 - \frac{\varepsilon_v(t)}{\varepsilon_1(t)}\right] dt}{2t_0} \tag{8}$$

where t_0 is the time point of axial strain at 0.5%. The mean value of the Poisson's ratio v_{mean} for the columnar ice is 0.324, 0.331, 0.328 under three temperature conditions, respectively. It means that the effect of temperature in the transverse dilatancy property of the columnar ice is insignificant. The peak points of volumetric strain are regarded as the demarcation point of elastic and plastic region, and the value of the radial dilatancy deformation is more than the value of the axial compression deformation since plastic behavior in the post-peak stage. In other words, the peak point of the volumetric strain is corresponding to the multiaxial yield point of ice sample under different complex stress states. It is worth emphasizing that the value of axial strain at the yield stress point (the peak point of the volumetric strain) belongs to the range of 0.5 ± 0.01% for the different loading conditions, as shown in Fig. 4(b). Therefore, the stress values at axial strain of 0.5% are defined as the multiaxial yield point of the columnar ice in this paper.

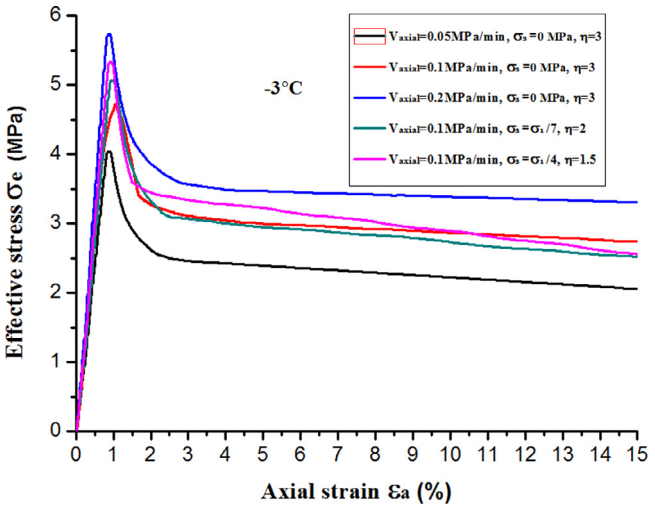

Fig. 5. Triaxial test results at different loading rates and loading paths.

Typical effective stress–axial strain curves of the columnar ice under different load rate and load path conditions are shown in Fig. 5. The shape of uniaxial ($\eta = 3$) and triaxial ($0 < \eta \leqslant 3$) curves has no significant difference, but the effects of stress rate and stress path in the curve level are considerable. Mean stress-volumetric strain responses at hydrostatical compression tests are summaried in Fig. 6. The curve for three temperatures all have such characteristics as an initial linear elastic region, a yield stress point, a short plateau region where the stress increases slowly as the pore compression plastically, and a densification region where stress increases rapidly. The ice sample is within the range of 0.86–0.9 g/cm^3 at three temperatures (−1.5 °C, −3 °C and −5 °C). Considering to the density of the pure ice (0.9 g/cm^3), the porosity of ice sample should range from 1 to 4%. Therefore, the ice sample under hydrostatic compression tests has undergone an initial elastic stage and pore compaction stage. The ice grain is subjected firstly to elastic deformation unit that the weakest pore is crushed, then the corresponding stress point is the hydrostatic yield strength. The other pores are continuously compressed in the plateau stage of stress–strain curves, as show in the Fig. 6. Then the ice grain has not recrystallized timely to form stable state as pores are sequentially crushed. Further increase of the hydrostatic pressure makes the crack initiation and propagation in the internal microstructure of ice sample (damage evolution), which can lead directly to continuously increase of volume strain (compaction process), as shown in plateau stage of Fig. 6. A comparison between the uniaxial and hydrostatic compression results indicates that the hardening rate under uniaxial compression is much hydrostatic compression. This implies the anisotropic hardening characteristics of the columnar ice are verified experimentally. In addition, the value of the uniaxial yield stress is clearly more than the hydrostatic yield stress under corresponding temperatures.

The initial yield surfaces of the columnar ice under different testing conditions are plotted in the stress space of the effective stress σ_e versus the mean stressσ_m, as shown in Fig. 7. It is clear that the experimental yield surfaces remain elliptical shape in the $\sigma_e - \sigma_m$ stress plane and show no evidence of corner development at all multiaxial yield points. It should be noted that the procedure of exploring experimental yield surface of the columnar ice was also executed by starting at the uniaxial loading path and gradually building up the hydrostatic pressure. This alternative testing method gave no substantial difference in the shape and size of experimental yield surface, and it demonstrates that the accumulated plastic-strain during the loading-unloading process has a negligible effect in the measured multiaxial yield points.

Therefore, a simple phenomenological yield criterion is proposed for the yield envelope surface of the columnar ice:

$$f = \sigma_e^2 + Y\left(T, \dot{\varepsilon}_{ij}, \varepsilon_{ij}^p\right)\sigma_m^2 - H\left(T, \dot{\varepsilon}_{ij}, \varepsilon_{ij}^p\right) = 0 \tag{9}$$

where σ_m and σ_e are the mean stress and the effective stress, respectively.$Y(T, \dot{\varepsilon}_{ij}, \varepsilon_{ij}^p)$ and $H(T, \dot{\varepsilon}_{ij}, \varepsilon_{ij}^p)$ are shape and size parameters (hardening parameters) as function of temperature, strain rate (stress rate) tensor and plastic strain tensor. Two parameters can be directly solved by using the uniaxial and hydrostatic yield stresses obtained from testing results (Table 1). The evolution of parameters is closely related to the experimental loading conditions. $H^{\frac{1}{2}}(T,\dot{\varepsilon}_{ij}, \varepsilon_{ij}^p)$ can be considered as the shear strength value of ice sample, and $[H(T,\dot{\varepsilon}_{ij}, \varepsilon_{ij}^p)/Y(T,\dot{\varepsilon}_{ij}, \varepsilon_{ij}^p)]^{\frac{1}{2}}$ can be regarded as the hydrostatic strength value of ice sample. It means that the effect of experimental conditions, such as temperature, loading path and rate, in the yield surface evolution can be attributed to the effect of those factors into the two failure mechanism. It is evident that the phenomenological yield criterion is capable of giving an approximate prediction for the experimental yield surface of the columnar ice over the investigated ranges of temperature and stress rate. The expansion of the experimental yield surface is almost isotropic from the low to high temperature, as shown in Fig. 7. It suggests that the multiaxial yield points at different stress states follow to the same

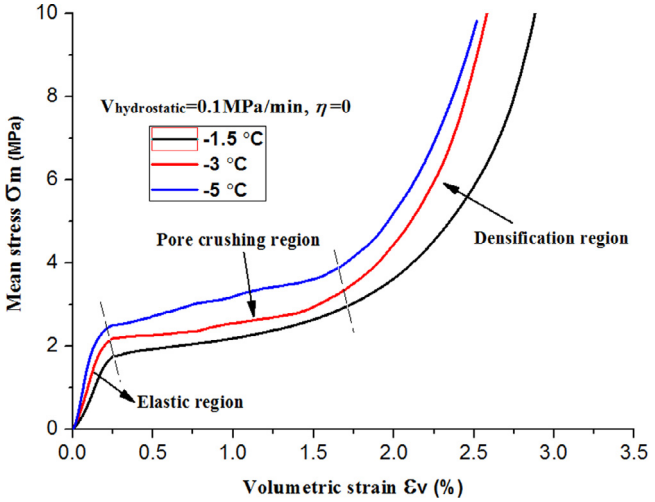

Fig. 6. Hydrostatic compression results at different temperatures.

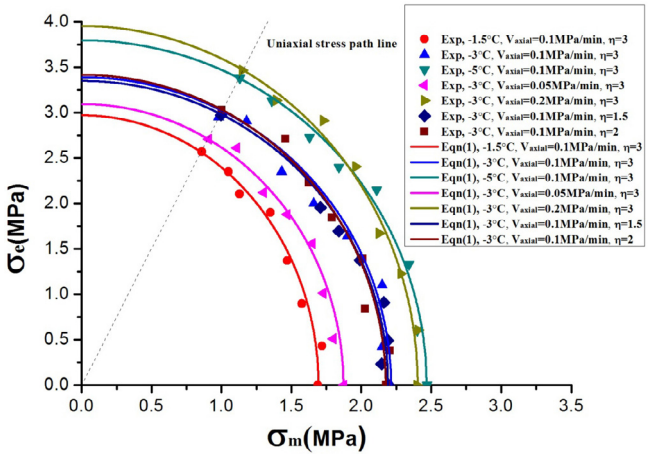

Fig. 7. Initial yield surface under different conditions.

Table 1
The value of two hardening parameters under different conditions.

Temperature T (°C)	Axial compression rate *Vaxial* (MPa/min)	Loading ratio η	Pre-strainε_1 (%)	Pre-strain ε_v (%)	Hardening parameter H	Hardening parameter Y
−1.5	0.1	3	0	0	0.76151	0.26663
−3	0.1	3	0	0	0.98185	0.20103
−5	0.1	3	0	0	1.3073	0.21428
−3	0.05	3	0	0	0.85033	0.24161
−3	0.2	3	0	0	1.35714	0.23573
−3	0.1	1.5	0	0	1.0152	0.21033
−3	0.1	2	0	0	1.02814	0.21632
−3	0.1	3	3	0	1.09217	0.20801
−3	0.1	3	6	0	1.32048	0.19778
−3	0.1	3	9	0	1.78865	0.23888
−3	0.1	3	12	0	2.44996	0.29736
−3	0.1	1.5	6	0	1.21025	0.18467
−3	0.1	2	6	0	1.11823	0.16328
−3	0.1	1.5	12	0	2.01154	0.23668
−3	0.1	2	12	0	1.83929	0.21897
−3	0.1	3	0	1	0.99666	0.15208
−3	0.1	3	0	1.5	0.99261	0.11484
−3	0.1	3	0	2	0.98894	0.08119
−3	0.1	3	0	2.5	0.98755	0.06839
−3	0.1	1.5	0	1.5	0.89389	0.10484
−3	0.1	2	0	1.5	0.85571	0.099
−3	0.1	1.5	0	2	0.88971	0.06227
−3	0.1	2	0	2	0.90874	0.06228

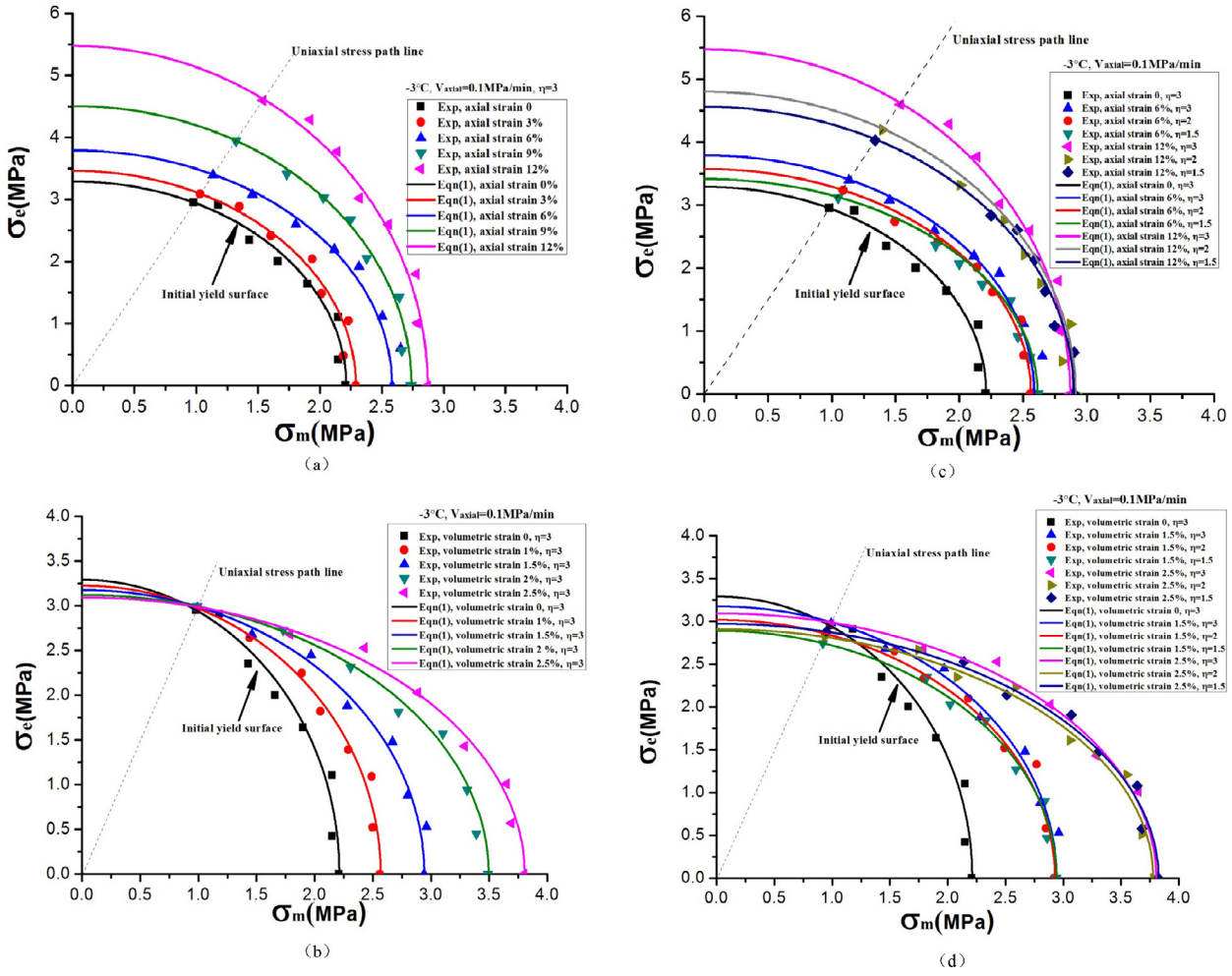

Fig. 8. Subsequent yield surface. (a) Uniaxial path. (b) Hydrostatic path. (c) Effect of loading path in uniaxial case. (d) Effect of loading path in hydrostatic case.

variation rule with temperature changes. The theoretical yield surface under different temperatures might be derived by using the enhancing ratio of the uniaxial yield stress and current yield criterion. The notable growth of the experimental yield surface as increasing of stress rate is validated, but the expansion ratio of the yield surface along the axis of the effective stress σ_e is distinctly more than along the axis of the mean stress σ_m. The primary reason for this difference is that the hardening behavior, induced by the rate effect, is anisotropic. Furthermore, the initial yield surfaces probed by three loading path are also shown in Fig. 7. The size and shape of the initial yield surface have an inappreciable variation, and the initial yield surface is insensitive to loading path.

Two stress paths, namely uniaxial and hydrostatic path, were selected for establishing the subsequent yield surfaces at pre-strain and further investigate the hardening characteristic of the columnar ice, as shown in Fig. 8. It can be found that the subsequent yield surfaces maintain ellipse shape under both two stress paths. And there is still no apparently corner development for all experimental yield surfaces. By excluding the pre-strain of 9% and 12%, subsequent yield surface approximately strengthens in an isotropic or geometrically self-similar pattern under uniaxial stress path condition, as shown in Fig. 8(a). The enhancing rate of the effective stress is gradually more as continued increase of the uniaxial strain. A possible reason for this interesting dissimilarity is that hardening rate with respect to different direction is not identically dependent on the axial strain in the stress space of effective stress versus mean stress. In the case of hydrostatic path, the subsequent yield surface prolongs remarkably toward the axis of the mean stress, and shrinkage slightly along the axis of the effective stress, as shown in Fig. 8(b). This unidirectional extension of subsequent yield surface occurs, because the hydrostatic path (volumetric strain) has an ignorable influence in the hardening development of the effective stress direction (pure shear stress path). In other words, the subsequent yield (hardening) behavior at the uniaxial and pure shear path does not rely in the change of the volumetric strain caused by the hydrostatic pressure. Because that the c-axes of this columnar ice sample are unaligned, this initial crystallographic structure leads directly to the anisotropy mechanical properties. The ice grain will recrystallize as the increases of the strain in the tests, and this recrystallization process of grain will induce further to the increase of the anisotropic degree. Therefore, the anisotropic hardening characteristic of columnar ice is dominated by the initial anisotropic microstructure and microstructural rearrangement induced by grain recrystallization. To better evaluate the coupling effect of the loading path and pre-strain in hardening rate, the subsequent yield surfaces obtained from three loading paths ($\eta = 1.5, 2, 3$) are drawn in Fig. 8(c) and (d). It can be seen that the evolution of yield surface is slightly sensitive to loading path. As the increasing of the loading ratio η, the yield surface has a little elongation along the axis of the effective stress. The main reason for this unidirectional hardening characteristic under the hydrostatic stress path is that the subsequent yield behavior of ice sample is dominated by the mean stress. The effect of loading path in the subsequent yield surfaces at pre-strain of 1.5% and 2.5% is insignificant under the hydrostatic stress path.

Conclusions

The triaxial compression tests, which is able to measure the volumetric strain of the sample, is performed on the columnar ice under different temperatures (−1.5 °C, −3 °C and −5 °C), loading rates (V axial = 0.05, 0.1, 0.2 MPa/min) and loading paths ($\eta = 1.5, 2, 3$) conditions. A new approach of exploring the experimental yield surface from a single sample was executed for studying the multiaxial yield and hardening behaviors of the columnar ice. The effect of temperature, loading rate and loading path in the initial and subsequent yield surface is also investigated experimentally. Some conclusions drawn from experimental and theoretical results are summarized below:

(1) The effects of temperature, loading rate and loading path in the shape of curves are negligible at the triaxial testing, but the curve level strongly depends on the aforementioned factors. The volumetric strain in triaxial tests ($0 < \eta \leqslant 3$) is distinctly composed of two parts, i.e. elastic compression stage and plastic dilatancy stage. Based on the characteristic of the volumetric strain, a new method of defined the multiaxial yield points of the columnar ice is proposed reasonably. The temperature effect in the Poisson's ratio of the columnar ice is insignificant.
(2) The experimental yield surfaces remain elliptical shape in the plane of effective stress versus mean stress, and show no evidence of corner development at all multiaxial yield points. The significant expansion of the initial yield surface with the temperature happens to be isotropic. Asymmetrical expansion of the initial yield surface as the increasing of the stress rate is validated experimentally. The initial yield surface of the columnar ice is not sensitive to the loading path.
(3) The subsequent yield surface maintains consistently elliptical shape under uniaxial and hydrostatic path. The evolution characteristic of the yield surface is geometrically self-similar pattern under uniaxial path, and the subsequent yield surface extends along the mean stress axis in the case of hydrostatic path. The hardening rate for the columnar ice under hydrostatic path is more than it uniaxial path. The anisotropic hardening behavior of the columnar ice is verified experimentally, and the size of subsequent yield surface relies strongly on the loading path.
(4) A phenomenological yield criterion for the columnar ice is presented in the stress space of effective stress versus mean stress. The theoretical envelope lines are approximate agreement with the experimental yield surfaces in the studied range of temperatures and loading rates. This simple but reliable theoretical model also has capable of predicting and describing to the subsequent yield surfaces in the case of uniaxial and hydrostatic paths.

Acknowledgements

This work was supported by the National key Basic Research Program of China under Grant 2012CB026106; National Natural Science Foundation of China under Grant (11502266, 41401077); Science and Technology Major Project of the Gansu Province under Grant 143GKDA007; West Light Foundation of the Chinese Academy of Sciences.

References

[1] Wu MS, Niu J. Micromechanical prediction of the compressive failure of ice: model development. Mech Mater 1995;20:9–32.
[2] Wu MS, Niu J. Micromechanical prediction of the compressive failure of ice: numerical simulations. Mech Mater 1995;20:33–58.
[3] Jordaan IJ, Matskevitch DG, Meglis IL. Disintegration of ice under fast compressive loading. Int J Fract 1999;97:279–300.
[4] Schulson EM, Gratz ET. The brittle compressive failure of orthotropic ice under triaxial loading. Acta Mater 1999;47:745–55.
[5] Singh SK, Jordaan IJ. Constitutive behaviour of crushed ice. Int J Fract 1999;97:171–87.
[6] Jordaan IJ. Mechanics of ice-structure interaction. Eng Fract Mech 2001;68:1923–60.
[7] Schulson EM. Brittle failure of ice. Eng Fract Mech 2001;68:1839–87.
[8] Schulson EM. Fracture of ice. Eng Fract Mech 2001;68:1793–5.

[9] Fortt AL, Schulson EM. The resistance to sliding along coulombic shear faults in ice. Acta Mater 2007;55:2253–64.
[10] Duval P, Montagnat M, Grennerat F, Weiss J, Meyssonnier J, Philip A. Creep and plasticity of glacier ice: a material science perspective. J Glaciol 2010;56:1059–68.
[11] Schulson EM, Fortt AL. Static strengthening of frictional surfaces of ice. Acta Mater 2013;61:1616–23.
[12] Taylor RS, Jordaan IJ. Probabilistic fracture mechanics analysis of spalling during edge indentation in ice. Eng Fract Mech 2015;134:242–66.
[13] Bassis JN, Walker CC. Upper and lower limits on the stability of calving glaciers from the yield strength envelope of ice. Proc R Soc A-Math Phys 2012;468:913–31.
[14] Ma W, Cheng GD, Wu QB, Wang DY. Application on idea of dynamic design in Qinghai-Tibet Railway construction. Cold Reg Sci Technol 2005;41:165–73.
[15] Ma W, Wu ZW, Zhang LX, Chang XX. Analyses of process on the strength decrease in frozen soils under high confining pressures. Cold Reg Sci Technol 1999;29:1–7.
[16] Xu XT, Lai YM, Dong YH, Qi JL. Laboratory investigation on strength and deformation characteristics of ice-saturated frozen sandy soil. Cold Reg Sci Technol 2011;69:98–104.
[17] Xu XT, Dong YH, Fan CX. Laboratory investigation on energy dissipation and damage characteristics of frozen loess during deformation process. Cold Reg Sci Technol 2015;109:1–8.
[18] Vasiliev NK, Pronk ADC, Shatalina IN, Janssen FHME, Houben RWG. A review on the development of reinforced ice for use as a building material in cold regions. Cold Reg Sci Technol 2015;115:56–63.
[19] Golden KM, Heaton AL, Eickenb H, Lytle VI. Void bounds for fluid transport in sea ice. Mech Mater 2006;38:801–17.
[20] Timco GW, Weeks WF. A review of the engineering properties of sea ice. Cold Reg Sci Technol 2010;60:107–29.
[21] Aryanpour G, Farzaneh M. Contribution of primary creep in modeling the mechanical behavior of polycrystalline ice. J Offshore Mech Arctic 2013;135:031502.
[22] Schulson EM, Duval P. Creep and fracture of ice. Cambridge University Press; 2009.
[23] Wachter LM, Renshaw CE, Schulson EM. Transition in brittle failure mode in ice under low confinement. Acta Mater 2009;57:345–55.
[24] Sain T, Narasimhan R. Constitutive modeling of ice in the high strain rate regime. Int J Solids Struct 2011;48:817–27.
[25] Duddu R, Waisman H. A temperature dependent creep damage model for polycrystalline ice. Mech Mater 2012;46:23–41.
[26] Golding N, Schulson EM, Renshaw CE. Shear localization in ice: mechanical response and microstructural evolution of P-faulting. Acta Mater 2012;60:3616–31.
[27] Tran HD, Sulsky DL, Schreyer HL. An anisotropic elastic-decohesive constitutive relation for sea ice. Int J Numer Anal Methods 2015;39:988–1013.
[28] Mellor M, Cole DM. Deformation and failure of ice under constant stress or constant strain-rate. Cold Reg Sci Technol 1982;5:201–19.
[29] Jones SJ. The confined compressive strength of polycrystalline ice. J Glaciol 1982;98:171–7.
[30] Nadreau JP, Michel B. Yield and failure envelope for ice under multiaxial compressive stresses. Cold Reg Sci Technol 1986;13:75–82.
[31] Nadreau JP, Nawwar AM, Wang YS. Triaxial testing of freshwater ice at low confining pressures. J Offshore Mech Arctic 1991;113:260–5.
[32] Timco GW, Freerking R. Confined compression tests-outlining the failure envelope of columnar sea ice. Cold Reg Sci Technol 1986;12:13–28.
[33] Smith TR, Schulson EM. Brittle compressive failure of salt-water columnar ice under biaxial loading. J Glaciol 1994;40:265–76.
[34] Rist MA, Murrell SAF. Ice triaxial deformation and fracture. J Glaciol 1994;40:305–18.
[35] Gagnon RE, Gammon PH. Triaxial experiments on ice-berg and glaciers ice. J Glaciol 1995;41:528–40.
[36] Gratz ET, Schulson EM. Brittle failure of columnar saline ice under triaxial compression. J Geophys Res 1997;102:5091–107.
[37] Derradji-Aouat A. Multi-surface failure criterion for saline ice in the brittle regime. Cold Reg Sci Technol 2003;36:47–70.
[38] Melton JS, Schulson EM. Ductile compressive failure of columnar saline ice under triaxial loading. J Geophys Res 1998;103:21759–66.
[39] Coon MD, Knoke GS, Echert DC. The architecture of an anisotropic elastic-plastic sea ice mechanics constitutive law. J Geophys Res 1998;103:21915–25.
[40] Sung SJ, Liu LW, Hong HK. Evolution of yield surface in the 2D and 3D stress spaces. Int J Solids Struct 2011;48:1054–69.
[41] Kabirian F, Khan AS. Anisotropic yield criteria in sigma-tau stress space for materials with yield asymmetry. Int J Solids Struct 2015;67–68:116–26.
[42] Castelnau O, Duval P, Montagnat M. Elastoviscoplastic micromechanical modeling of the transient creep of ice. J Geophys Res 2008;113:B11203.
[43] Castelnau O, Duval P, Lebensohn RA. Viscoplastic modeling of texture development in polycrystalline ice with a self-consistent approach: comparison with bound estimates. J Geophys Res 1996;101:13851–68.
[44] Kuehn GA, Lee RW, Nixon WA, Schulson EM. The structure and tensile behavior of first-year sea ice and laboratory grown saline ice. J Offshore Mech Arctic 1990;112:357–63.